Propagation dynamics of ultrabroadband terahertz beams with orbital angular momentum for wireless data transfer

Kulya, Maksim; Sokolenko, Bogdan; Gorodetsky, Andrei; Petrov, Nikolay

DOI:
10.1117/12.2547695

Document Version
Peer reviewed version

Propagation dynamics of ultrabroadband terahertz beams with orbital angular momentum for wireless data transfer

Maksim S. Kulya[1,2], Bogdan Sokolenko[1], Andrei Gorodetsky[1,3], and Nikolay V. Petrov[1]

[1]ITMO University, Digital and Display Holography Laboratory, St. Petersburg 197101, Russia
[2]Tampere University, Faculty of Information Technology and Communication, Tampere 33100, Finland
[3]School of Physics and Astronomy, University. of Birmingham, Birmingham B15 2TT, UK

ABSTRACT

We investigate an approach to short and medium-range wireless communications based on the use of terahertz beams possessing an orbital angular momentum (OAM) that allows for noise-resistant broadband carrier. A theoretical model of the proposed beams generation is developed and numerical predictions are given for propagation and visualization of complex-structured THz beams, including ones carrying a unit topological charge on a large number of spectral components of broadband terahertz radiation. The assessment method which in our case is terahertz pulse time-domain holography allows for analyzing spatio-temporal and spatio-spectral evolution of arbitrary shaped THz wave trains during their propagation in free space and interaction with obstacles.

Keywords: Vortex beams, THz radiation, wireless data transfer

1. INTRODUCTION

The growing need for high-speed telecommunications has become a problem that cannot be solved by only increasing the currently available technologies. The capacity of the data stream increases exponentially with time, and by the 2020 Internet traffic should have increased up to 170 exabytes/month.[1] The fastest growing part of this traffic is wireless communication channels, engaged by the activity of mobile device users that have already overtaken the amount of desktop Internet users traffic. Moreover, ultra high speed wireless communications are highly demanded in data centres,[2] as they are more energy efficient and can be faster than fibre links. Given the ultimate need for fast and reliable channels for wireless data transfer, the scale of this problem is global and fundamental.

One of the most natural approaches to raising the bandwidth of wireless radio communication channels is shifting the technology to the higher frequency band of the electromagnetic spectrum. A further increase in the carrier frequency and the bandwidth with radiophysical methods is complicated, and therefore, for development of wireless communication systems, it is reasonable to go up in frequency in the THz band. Both continuous[3] and pulsed[4,5] THz radiation that possesses a ultrabroad spectral bandwidth for even higher capacity are considered for these tasks.

With the exception of certain resonant frequencies, where exist strongly water vapor absorption, THz radiation has some obvious advantages for wireless data transfer not only over GHz/microwave range but also over IR and visible radiation because most common dielectric materials that are opaque for IR and visible (cardboards, plastic, wood) are transparent in this frequency range. One of the most significant obstacles for the implementation of broadband terahertz communication systems is the noise resulting from molecular absorption (mostly by water molecules, if run in Earth atmosphere) during its propagation. Apart from these, THz radiation is sensitive to the dynamic and static clutters, such as metallic barriers that block the transmission channel or optical density inhomogenuities in dielectric materials on the propagation axis resulting in beam scattering and generated speckle patterns.

Further author information: (Send correspondence to N.V.P.)
N.V.P.: E-mail: n.petrov@niuitmo.ru

Beams carrying the optical angular momentum (OAM) are proven to be more information-intensive, as they support OAM-based multiplexing of communication channels both in millimetre[6,7] and visible frequency ranges.[7,8] Moreover, they also possess self-restoration properties after collisions with opaque obstacles.[9,10]

This work addresses the use of pulsed broadband radiation for wireless telecommunications. While the issues of compact efficient generators and wave division multiplexing (WDM) are still outside this discussion, here we consider the generation of pulsed wave packets with broadband uniformly topologically charged (BUTCH) THz beams. We give their mathematical description and consider the features of the temporal and spectral structure of the field that occur during the generation of such beams for the case of topological charges of $\mathsf{L} = 1$ and $\mathsf{L} = 2$ for each spectral component. Then we analyze the field profiles for the case of superimposing such beams and study propagation dynamics from the point of view of stability of the structure of the forming (in a result of interference) spectral channels.

To study the beams, we use the THz pulsed time-domain holography (THz PTDH).[11–14] This technique not only allows for temporal analysis of the pulse field, but also to spatially resolve amplitude and phase characteristics of each spectral component. And such analysis can be run not only on the basis of the experimental data, but also upon numerical simulation of the propagation of the above mentioned beams in various environments.

2. SETUP FOR NUMERICAL SIMULATION

Figure 1 shows the elementary diagram of the setup for the two BUTCH THz beams multiplexing and subsequent numerical demultiplexing.

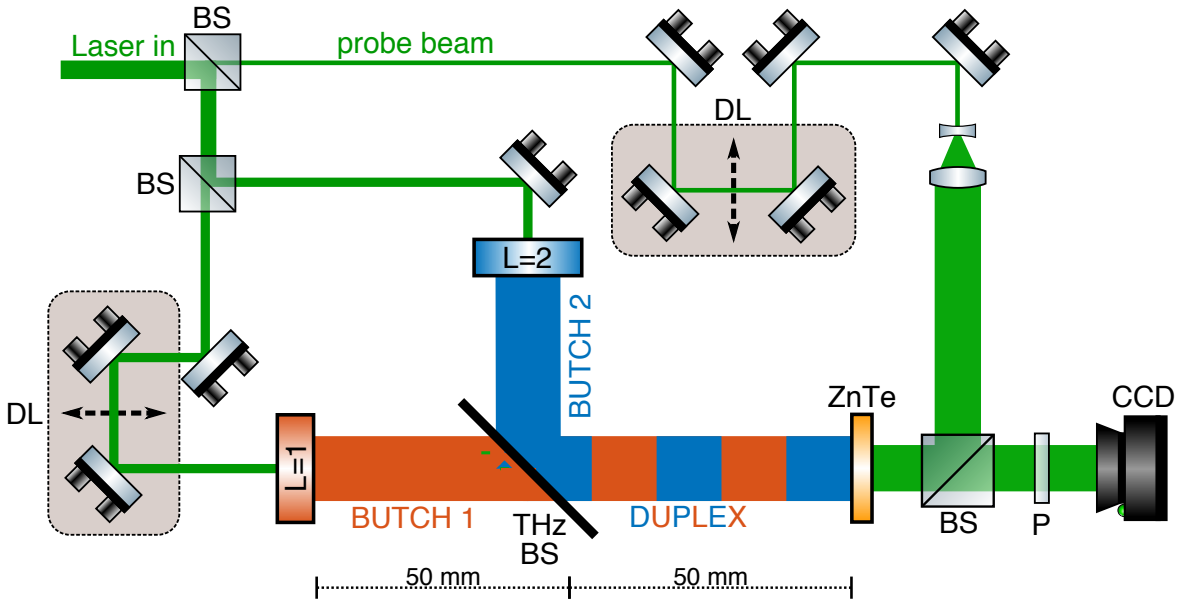

Figure 1. General layout of the simulation (not to scale). BS - beam splitter, THz - THz beam combiner, BUTCH 1 and BUTCH 2 - beams with topological charges $\mathsf{L} = 1$ and $\mathsf{L} = 2$, respectively, DUPLEX - multiplexed THz beam, ZnTe - electro-optic crystal for detection, P - polariser, CCD - camera, DL - mechanical delay line.

Input utrafast polarized laser radiation is split into the probe beam that is used for THz detection and the pump beam that is split again to generate two THz BUTCH beams with uniform charges of 1 and 2 across their spectra, as described below in section 3.1. These beams are overlayed with a THz beam combiner (semi-transparent plate, made of either polymer or hi-resistive silicon). Delay line in BUTCH 1 beamline controls the mutual position of the pulses in time.

Then, overlapped beams evolve during diffractive propagation which is investigated by a coherent electro-optic detection scheme, described in detail elsewhere.[15] Independently delayed probe beam scans the wavefront in time-domain. As a result, spatially resolved time domain THz pulse profiles are recorded through the CCD.

3. GENERATION OF BROADBAND THZ BEAMS WITH ANGULAR ORBITAL MOMENTUM

3.1 BUTCH-beam

Implementing of birefringent crystals as a method for vector vortex beam generation with spatial polarization rotations at the local parts of input beam were introduced.[16,17] In this case, linearly or circularly polarised incident beam may be transformed to perform desired polarization pattern. Along with axially symmetric crystalline birefringent elements, the devices for spatial rotation of the separate beam areas were developed for THz range.[18] The choice of polarization type of incident beam on the input face of a such element is driven by its quarter- or half-wave retardation and, as result, the portion of orbital angular momentum could be introduced to a broadband THz beams. Optical elements which uses the mentioned principle to form desired polarization vortex state were called Pancharatnam–Berry phase optical elements[19–21] and utilises spin-to-orbital momentum conversion principle.[22]

Actually, THz BUTCH beam is not a very obvious structure – however there is an experimental approach that allows for its direct generation.[23] To obtain a BUTCH beam, radially polarized THz pulses are sent through the achromatic quarter-wave plate, where polarization acquires different ellipticity. Thus, in the output of a polariser placed after the waveplate, the phase of the beam gets linearly modulated with respect to the angular beam coordinate θ. The discontinous jump of the phase in the beam crossection equal to $2\pi\mathsf{L}$ denotes the presence of the topological charge of L in the beam. And such charge accrued is the same for every component of the THz pulse spectrum.[10] Spatio-temporal beam shapes for simulated THz BUTCH beams with charges $\mathsf{L} = 1$ and $\mathsf{L} = 2$ are shown in Figure 2.

The spatial amplitude and phase distributions for selected frequency component 0.5 THz are shown in Figure 2 in the top row for THz BUTCH beams with topological charges 1 and 2. Middle row shows time-dependent electrical field amplitude for the two selected points in the spatial amplitude distribution of the vortex pointed by 1 and 2. Note, that beam with charge 2 is has time delay due to the fact that it corresponds to the delayed initial pulse. Bottom rows also illustrate the time-of-flight field distribution at fixed time scale, showing the rotation of such vortex beam temporal shape. The vortex structure in Figure 2 proves the spatio-temporal and spatio-spectral cross-coupling previously observed in ultrashort pulses.[24]

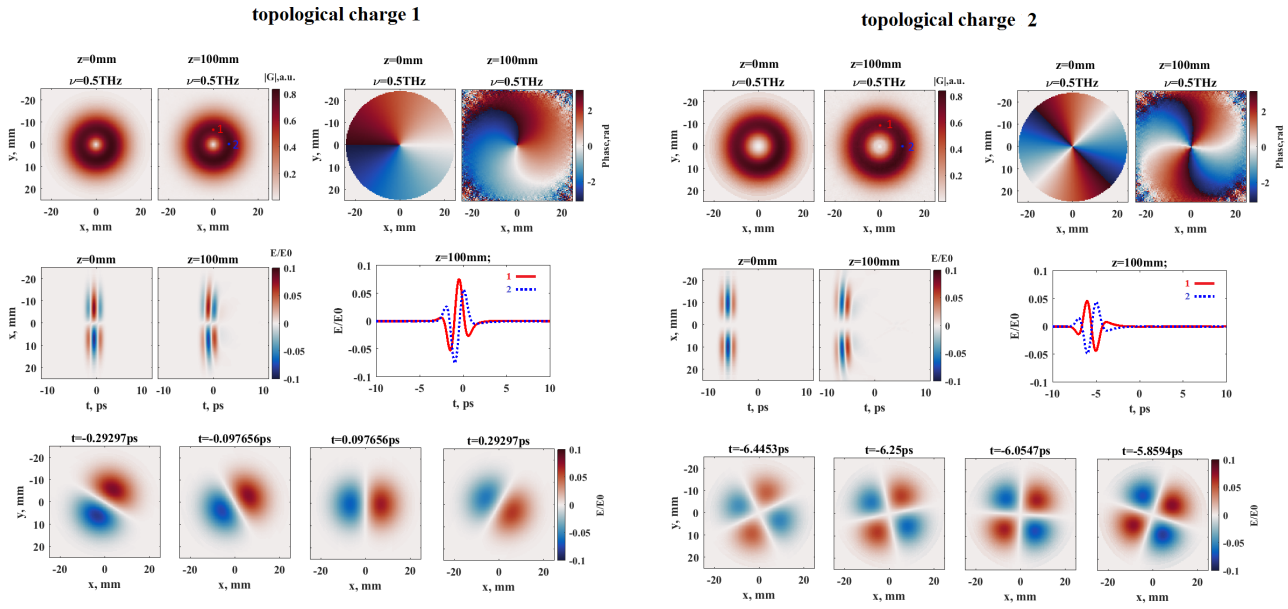

Figure 2. THz BUTCH beam structure with topological charges $\mathsf{L} = 1$ and $\mathsf{L} = 2$.

3.2 Vector vortex beam shaping with q-plates

To introduce spiral wavefront into a THz-beam let us consider the transformations exhibited by the Jones matrix of a circularly polarized wave propagating orthogonal to the optical axis of a media with nonuniform anisotropy.[16] The input uniformly circularly polarised beam is assumed to have the components $M = \frac{1}{\sqrt{2}}\begin{pmatrix}1\\ i\sigma\end{pmatrix}$, where $\sigma = \pm 1$ denotes right $(-)$ or left $(+)$ handedness of the electric vector circulation. Then, the Jones matrix for the uniaxial media or wave plate with arbitrary retardation δ can be written as:

$$J = \begin{bmatrix} \cos\frac{\delta}{2} - i\sin\frac{\delta}{2}\ \cos 2\alpha & -i\sin\frac{\delta}{2}\ \sin 2\alpha \\ -\sin\frac{\delta}{2}\ \sin 2\alpha & \cos\frac{\delta}{2} + i\sin\frac{\delta}{2}\ \cos 2\alpha \end{bmatrix}, \tag{1}$$

where α is the angle of optical axis orientation against the x direction. When optical axis of the wave plate is tilted at the angle $\alpha \neq 0$ to the direction of incident beam polarization, the output beam polarization will exhibit rotation at 2α relatively to the direction of incident polarization. In case of quarter-wave plate, the retardation is $\delta = \frac{\pi}{2}$ and one gets the Jones matrix in the form:

$$J_{\frac{\lambda}{4}} = \frac{1}{\sqrt{2}}\begin{bmatrix} 1 - i\cos 2\alpha & -i\sin 2\alpha \\ -i\sin 2\alpha & 1 + \cos 2\alpha \end{bmatrix}. \tag{2}$$

Most widely used topological shaping devices for THz pulses basically utilise a half-wave quartz birefringent plate $(\delta = \pi)$, whose Jones matrix may be expressed as:

$$J_{\frac{\lambda}{2}} = \begin{bmatrix} \cos 2\alpha & \sin 2\alpha \\ \sin 2\alpha & -\cos 2\alpha \end{bmatrix}. \tag{3}$$

To perform Pancharatnam–Berry geometric phase shaping, optical axis angle α in the (x,y) plane should exhibit a uniform distribution over the whole surface of anisotropic plate, which is given by the following relation:[21] $\alpha(\mathsf{y},\mathsf{x}) = q\varphi + \alpha_0$, where $\varphi = \arctan(\mathsf{y}/\mathsf{x})$ is the azimuthal angle in the (x,y) plane, q is an integer or semi-integer constant and α_0 denotes arbitrary value. In this way, the polarization of wave is experiencing a continuous sequence of spatial turns which were determined by value q, hence, the slab with non-uniform anisotropy in its separate parts was called q-plate[20,22] and designed in various constructive solutions.[16,25–28] In practice, we may restrict ourselves to the q-plate with half-wave retardation so that orientations of optical axes have a local defect only at its center without discontinuity elsewhere on a plate. The plates with $q = 1/2$ and $q = 1$ give rise to a uniform wavefront modulation given by $\theta = \pm 2q\varphi$ and thus helical vortex structure with topological charge $\mathsf{L} = \pm 2q$ originates. The handedness of the vortex phase helicity and a sign of topological charge are controlled by polarization circularity σ of input field: $\mathrm{sign}(\mathsf{L}) = \mathrm{sign}(\sigma)$.

Substituting an expression for the q-plate transformation law into the Jones matrix (eq. (3)), we can convert an initial wave field with, in particular, with left-hand circular polarisation into the output field with a vector vortex on the beam axis in orthogonal polarization component:

$$E_{out}(x,y,z) = \Psi(x,y,z)\, J_{\frac{\lambda}{2}} M = \Psi \exp\left[\pm i2\left(q\varphi \pm \alpha_0\right)\right] M^*, \tag{4}$$

where $(*)$ denotes complex conjugation and $\Psi(x,y,z)$ is the scalar amplitude of the input field. Without loss of generality, we can assume the amplitude of incoming beam to be Gaussian envelope with beamwaist radius ω_0 on the input face of the q-plate and Rayleigh length $z_r = k\omega_0^2/2$:

$$\Psi(x,y,z) = \exp\left(-\frac{x^2+y^2}{\omega^2}\right)\exp\left(-i\frac{\pi\left(x^2+y^2\right)}{z\left[1+\left(\frac{z_r}{z}\right)\right]^2\lambda}\right), \tag{5}$$

where ω is a beamwaist at the distance z from the waist plane and (x,y,z) are Cartesian coordinates. After substituting Gaussian envelope into the eq. (4), where, for simplicity, we assume $\alpha_0 = 0$, the equation for output

circularly polarized vortex field can be written explicitly:

$$E_{out}(x,y,z) = \frac{1}{\sqrt{2}} \exp\left(-\frac{x^2+y^2}{\omega^2}\right) \exp\exp\left(-i\frac{\pi\left(x^2+y^2\right)}{z\left[1+\left(\frac{z_r}{z}\right)\right]^2\lambda}\right) \exp\left[\pm i\mathsf{L}\arctan\left(\frac{y}{x}\right)\right]\begin{pmatrix}1\\-i\sigma\end{pmatrix} \tag{6}$$

As it was shown [29] for the q-plates there occurred complete conversion between right or left circular polarization components of the incident light after half-wave retardation on a specific wavelength λ_0. When a light beam, which wavelength λ differs from the wavelength the q-plate was designed for, during the propagation through a q-plate, only part of this beam in opposite circular polarisation component is transformed into a vortex beam, while another part with initial polarisation state remains unchanged. Thereby, an achromatic q-plate may be employed to broadband vector vortex beam generation with certain purity which directly affects on conversion efficiency.

4. PROPERTIES OF MULTIPLEXED SIGNALS

Here, we present the properties of the beam resulting from the overlap of the two THz BUTCH beams with charges $\mathsf{L} = 1$ and $\mathsf{L} = 2$. Beam time domain profiles and spatial cross sections at different timestaps for two different relative pulse delays at the propagation distance of 100 mm from each BUTCH beam generator are shown in Figure 3.

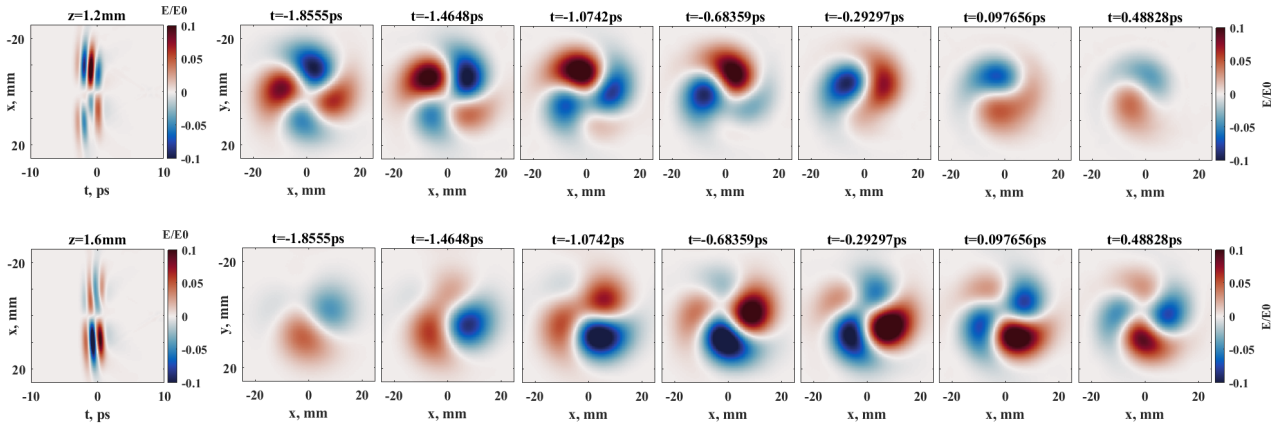

Figure 3. Spatio-temporal profiles for two cases of overlapped BUTCH beams and time-of-flight images.

The results are shown for two delay positions corresponding to the maximum amplitude of the total field over the entire beam. Two delay positions were found to provide this maximum: first case (shown in the top row of the Figure 3, delay is equal to 1.2 mm, that corresponds to 4 ps). Delayed pulse has not yet reached the middle of the beam 2 in the temporal coordinates. The second position (bottom row) corresponds to the delayed pulse arriving earlier.

Their corresponding spatio-spectral distributions and spatial cross-sections of the spectral amplitudes of the outlined components are shown in Figure 4.

In the first row, the spectum and cross-sections for the two pulses separated by the delay of 0 mm are shown. In the first column, the result of the interference of two delayed beams is depicted, and it reveals that broadband frequency comb is formed. Earlier, similar combs were reported, and they were obtained using the overlap of the two THz pulses shifted in time.[5] It is proposed that one can create a frequency comb for data transfer, where the channel width is set by the delay between pulses. In the case of flat wave fronts, it is uniform in space. In the case of vortex wave fronts, they are spatially dependent. Since there are 2 different vortices (BUTCH 1 and BUTCH 2), the "comb" in the figure (upper left corner) will be inhomogeneous in space because it has uneven spectral periods.

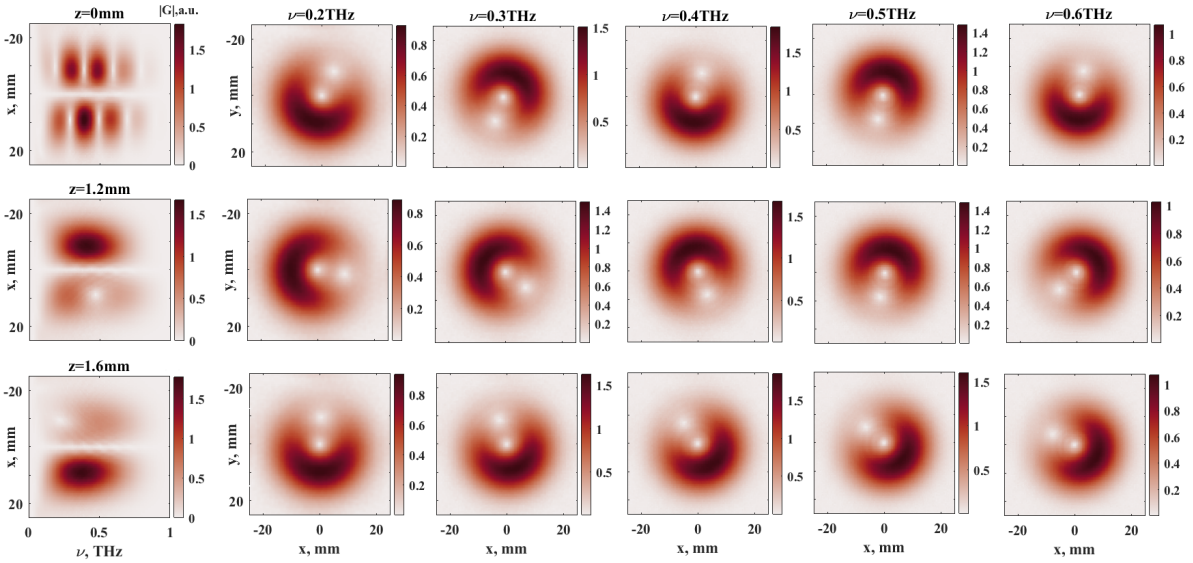

Figure 4. Amplitude spectrum of two multiplexed BUTCH beams at different time delay corresponded to propagation distances 0 mm, 1.2 mm and 1.6 mm for the beam with charge 2. First column is the spatio-spectral representation for central cross-section of the beam. Other columns shows spatial distribution of the spectrum for several frequencies.

When the delay between the beams is 5 ps, the half-turn is done at 0.1 THz. The delay of -1 ps (1.2 mm) corresponds to the half a turn at 0.6 THz (between 0.2-0.8 THz). When the delay is 1.6 mm (+0.3 ps), a quarter turn is done at 0.6 THz (between 0.2-0.8 THz), and in this case, the rotation is already going in the other direction (counterclockwise when the frequency is increased).

5. CONCLUSION

In this work, we considered the concept of two BUTCH beams duplexing for further application in telecommunication systems. We described the physical principle of BUTCH beam generation, and gave its mathematical description. Using the THz PTDH method, we studied the spatio-spectral and spatio-temporal evolution of a complex wave packet formed with the two beams. An important conclusion made on the basis of the presented visualization is the difference between the spectral channels formed at beams' different spatial segments as a result of interference of two differently charged BUTCH beams. This effect allows one to use the comb formed thuswise as the basis for WDM-type compression. More rigorous analysis of the interdependence of the temporal and spatio-spectral structure can also provide new approaches to compression the transmitted data within the set of weakly correlated components.

Further research should include the development of simultaneous OAM and WDM compression technologies, and the development of a detection system specification followed by the analysis of noise and interference immunity during the registration and decoding. We believe that the information obtained in the result of this study will find application in the development of wireless telecommunications systems with pulsed broadband terahertz radiation.

Development of technologies and means for telecommunication using broadband THz communication channels will allow for solving multiple important tasks, such as transferring large amounts of data through a wireless communication between two devices, including mobiles, servers and spacecrafts. This will lead to the emergence of new technologies, currently limited by currently existing transmission systems bandwidth. Among the examples of such applications are: instant reading of large data arrays that contain biometric information from mobile devices, data exchange between portable virtual reality systems, wireles data center connections, and realtime high-quality communication between spaceships. Provision of high speed wireless data links is important for transmission of real-time streams of audio and video, cloud computing, data centers and business applications. An important application is the transfer of data within computing systems via a wireless bus, which provides

communication between external hard drives and wireless monitors. Local wireless high speed network is not the only possible application of THz photonics in telecommunications. By using more powerful sources of THz radiation, in principle, it is possible to create channels of communication with high speed data transfer between space satellites and other objects in the airless environment.

ACKNOWLEDGMENTS

The work was supported by Russian Science Foundation, Project No 19-72-10147.

REFERENCES

[1] Nagatsuma, T., Ducournau, G., and Renaud, C. C., "Advances in terahertz communications accelerated by photonics," *Nat. Photonics* **10**(6), 371–379 (2016).

[2] Arnon, S., "Optical wireless communication in data centers," *Proc. SPIE* **10559**, 105590J (2018).

[3] Oshima, N., Hashimoto, K., Suzuki, S., and Asada, M., "Terahertz Wireless Data Transmission With Frequency and Polarization Division Multiplexing Using Resonant-Tunneling-Diode Oscillators," *IEEE Trans. Terahertz Sci. Technol.* **7**, 593–598 (sep 2017).

[4] Semenova, V. and Bespalov, V., "Terahertz Technologies for Telecommunications," *Photonics* **51**(3), 126–141 (2015).

[5] Grachev, Y. V., Liu, X., Putilin, S. E., Tsypkin, A. N., Bespalov, V. G., Kozlov, S. A., and Zhang, X.-C., "Wireless data transmission method using pulsed thz sliced spectral supercontinuum," *IEEE Photon. Techol. Lett.* **30**(1), 103–106 (2017).

[6] Yan, Y., Xie, G., Lavery, M. P. J., Huang, H., Ahmed, N., Bao, C., Ren, Y., Cao, Y., Li, L., Zhao, Z., Molisch, A. F., Tur, M., Padgett, M. J., and Willner, A. E., "High-capacity millimetre-wave communications with orbital angular momentum multiplexing," *Nat. Commun.* **5**(1), 4876 (2014).

[7] Ahmed, N., Zhao, Z., Li, L., Huang, H., Lavery, M. P. J., Liao, P., Yan, Y., Wang, Z., Xie, G., Ren, Y., Almaiman, A., Willner, A. J., Ashrafi, S., Molisch, A. F., Tur, M., and Willner, A. E., "Mode-Division-Multiplexing of Multiple Bessel-Gaussian Beams Carrying Orbital-Angular-Momentum for Obstruction-Tolerant Free-Space Optical and Millimetre-Wave Communication Links," *Sci. Rep.* **6**(1), 22082 (2016).

[8] Wang, J., Yang, J.-Y., Fazal, I. M., Ahmed, N., Yan, Y., Huang, H., Ren, Y., Yue, Y., Dolinar, S., Tur, M., and Willner, A. E., "Terabit free-space data transmission employing orbital angular momentum multiplexing," *Nat. Photonics* **6**(7), 488–496 (2012).

[9] Mendoza-Hernández, J., Arroyo-Carrasco, M. L., Iturbe-Castillo, M. D., and Chávez-Cerda, S., "Laguerre–Gauss beams versus Bessel beams showdown: peer comparison," *Opt. Lett.* **40**(16), 3739 (2015).

[10] Kulya, M., Semenova, V., Gorodetsky, A., Bespalov, V. G., and Petrov, N. V., "Spatio-temporal and spatiospectral metrology of terahertz broadband uniformly topologically charged vortex beams," *Appl. Opt.* **58**(5), A90 (2019).

[11] Petrov, N. V., Gorodetsky, A. A., and Bespalov, V. G., "Holography and phase retrieval in terahertz imaging," *Proc. SPIE* **8846**, 88460S (2013).

[12] Petrov, N. V., Kulya, M. S., Tsypkin, A. N., Bespalov, V. G., and Gorodetsky, A., "Application of Terahertz Pulse Time-Domain Holography for Phase Imaging," *IEEE Trans. Terahertz Sci. Technol.* **6**(3), 464–472 (2016).

[13] Kulya, M., Petrov, N. V., Katkovnik, V., and Egiazarian, K., "Terahertz pulse time-domain holography with balance detection: complex-domain sparse imaging," *Appl. Opt.* **58**(34), G61–G70 (2019).

[14] Kulya, M. S., Balbekin, N. S., Gorodetsky, A., Kozlov, S. A., and Petrov, N. V., "Vectorial terahertz pulse time-domain holography for broadband optical wavefront sensing," *Proc. SPIE* , (to be published) (2020).

[15] Balbekin, N. S., Kulya, M. S., Belashov, A. V., Gorodetsky, A., and Petrov, N. V., "Increasing the resolution of the reconstructed image in terahertz pulse time-domain holography," *Sci. Rep.* **9**(1), 180 (2019).

[16] Shu, W., Ling, X., Fu, X., Liu, Y., Ke, Y., and Luo, H., "Polarization evolution of vector beams generated by q-plates," *Photonics Res.* **5**(2), 64 (2017).

[17] Karpeev, S. V., Podlipnov, V. V., Khonina, S. N., Paranin, V. D., and Reshetnikov, A. S., "A four-sector polarization converter integrated in a calcite crystal," *Computer Optics* **42**(3), 401–407 (2018).

[18] Minasyan, A., Trovato, C., Degert, J., Freysz, E., Brasselet, E., and Abraham, E., "Geometric phase shaping of terahertz vortex beams," *Opt. Lett.* **42**(1), 41 (2017).

[19] Hasman, E., Kleiner, V., Biener, G., and Niv, A., "Phase Optics: Formation of Pancharatnam- Berry Phase Optical Elements With Space-Variant Subwavelength Gratings," *Opt. Photonics News* **13**(12), 45 (2002).

[20] Biener, G., Niv, A., Kleiner, V., and Hasman, E., "Formation of helical beams by use of Pancharatnam–Berry phase optical elements," *Opt. Lett.* **27**(21), 1875 (2002).

[21] Marrucci, L., Manzo, C., and Paparo, D., "Pancharatnam-Berry phase optical elements for wave front shaping in the visible domain: Switchable helical mode generation," *Appl. Phys. Lett.* **88**(22), 221102 (2006).

[22] Marrucci, L., Manzo, C., and Paparo, D., "Optical spin-to-orbital angular momentum conversion in inhomogeneous anisotropic media," *Phys. Rev. Lett.* **96**(16), 1–4 (2006).

[23] Imai, R., Kanda, N., Higuchi, T., Konishi, K., and Kuwata-Gonokami, M., "Generation of broadband terahertz vortex beams," *Opt. Lett.* **39**(13), 3714–3717 (2014).

[24] Akturk, S., Gu, X., Bowlan, P., and Trebino, R., "Spatio-temporal couplings in ultrashort laser pulses," *J. Opt.* **12**(9) (2010).

[25] Slussarenko, S., Murauski, A., Du, T., Chigrinov, V., Marrucci, L., and Santamato, E., "Tunable liquid crystal q-plates with arbitrary topological charge," *Optics Express* **19**(5), 4085 (2011).

[26] Naidoo, D., Roux, F. S., Dudley, A., Litvin, I., Piccirillo, B., Marrucci, L., and Forbes, A., "Controlled generation of higher-order Poincaré sphere beams from a laser," *Nat. Photonics* **10**(5), 327–332 (2016).

[27] Ji, W., Lee, C.-H., Chen, P., Hu, W., Ming, Y., Zhang, L., Lin, T.-H., Chigrinov, V., and Lu, Y.-Q., "Meta-q-plate for complex beam shaping," *Sci. Rep.* **6**(1), 25528 (2016).

[28] Larocque, H., Gagnon-Bischoff, J., Bouchard, F., Fickler, R., Upham, J., Boyd, R. W., and Karimi, E., "Arbitrary optical wavefront shaping via spin-to-orbit coupling," *Journal of Optics* **18**(12), 124002 (2016).

[29] Gecevicius, M., Ivanov, M., Beresna, M., Matijosius, A., Tamuliene, V., Gertus, T., Cerkauskaite, A., Redeckas, K., Vengris, M., Smilgevicius, V., and Kazansky, P. G., "Toward the generation of broadband optical vortices: extending the spectral range of a q-plate by polarization-selective filtering," *J. Opt. Soc. Am. B* **35**(1), 190 (2018).